Composite Structures 124 (2015) 228–235

Contents lists available at ScienceDirect

Composite Structures

journal homepage: www.elsevier.com/locate/compstruct

Thermal buckling of composite plates with spatial varying fiber orientations

A.V. Duran [1], N.A. Fasanella [1], V. Sundararaghavan *, A.M. Waas [1]

University of Michigan, 1320 Beal Ave, 3025 FXB Building, Ann Arbor, MI 48109, USA

ARTICLE INFO

Article history:
Available online 13 January 2015

Keywords:
Laminates
Thermal buckling
Variable stiffness
Composite plates

ABSTRACT

Thermal buckling analysis of square composite laminates with variable stiffness properties is presented. Fiber angles vary spatially and result in material properties that are functions of position. The thermal critical buckling temperatures for such laminates are obtained numerically based on classical lamination theory and the finite element method. In this work, the domain is discretized to transform nonlinear fiber path functions to linear piecewise functions. Using this method, thermal responses for symmetric balanced laminates under constant thermal load is investigated and the optimal fiber paths to resist thermal buckling are obtained for multiple material models. The coefficients of thermal expansion are varied to study the effect on the critical buckling temperature and optimal fiber path. Validation for the method presented is achieved using the results for the special case of constant fiber angles found in literature. This work finds curved fiber path configurations that provide a 36.9% increase of resistance to thermal buckling in comparison to straight fiber configurations.

1. Introduction

High speed aircrafts and space systems are subject to severe aerodynamic heating and vastly changing thermal environments during flight. To maintain, structural integrity under high temperature environments, vehicle structural design concepts must differ from those of low Mach number aircraft. In particular, management of high thermal stresses that occur during high speed flight involve development of materials that can withstand thermal bucking. Response of composite panels in compression (due to thermal loading and edge restraints) is a classical plate buckling problem. Earlier works have shown that composite laminates offer superior buckling performance when compared to isotropic plates. For square laminates with simply supported boundary conditions the optimal angle-ply layup is reported as $[\pm 45]_{ns}$ [1–3].

However, current technology allows us to relax the assumption that the fibers be straight for each layer in a laminated fiber composite. Advanced manufacturing techniques, such as fiber steering, allow fibers to be oriented along a desired path. Variable fiber path laminates produce unique boundary conditions that produce local transverse and compressive stresses which develop simultaneously [4]. These stress fields may be exploited to increase buckling resistance in local areas where panels tend to buckle. Towards this end, Gürdal and Olmedo [5–7] have developed material models for variable stiffness composites and have continued to, along with others, develop models for in-plane and buckling responses. Groh and Weaver [8] extended these ideas into a three-dimensional form by varying the thickness of the panel and including the effects of shear deformation.

Optimization methods and techniques have been applied to these complex material systems. Hyer and Charette [10] use local optimization where the fiber angle varies over each element. In their work, they calculate the stress at each element and locally align fibers with the principal stress direction. Both Setoodeh et al. [12] and IJsselmuiden et al. [13] optimize the fiber angle locally at each node with respect to buckling and stiffness. As a result IJsselmuiden et al. investigate the trade off between buckling and stiffness. Alternatively, one could also optimize the fiber angle using a global parameterization of the fiber path. Nagendra et al. [11] use a basis shape optimization approach to maximize critical buckling load for a plate with a hole. Similarly, Jegley et al. [9] optimize a curvilinear fiber path for a plate with a hole. In their work, they minimize stress concentrations using genetic discrete-valued optimizer. Alternatively by minimizing the total thermal expansion, Rangarajan et al. [1] have shown that straight fibers paths

* Corresponding author at: Dept. of Aerospace Engineering.
E-mail addresses: avduran@umich.edu (A.V. Duran), nickfas@umich.edu (N.A. Fasanella), veeras@umich.edu (V. Sundararaghavan), dcw@umich.edu (A.M. Waas).
[1] Address: Dept. of Aerospace Engineering.

http://dx.doi.org/10.1016/j.compstruct.2014.12.065
0263-8223/

are the optimum configuration to minimize total thermal expansion along principal material directions. In their work, a constant strain state is assumed and results are obtained analytically. These studies have shown that variable stiffness laminates allow improved buckling performance in the order of four to six times that of isotropic panels [13].

Although structural buckling of variable stiffness panels has been intensively studied, numerical optimization approaches have not yet been applied for thermal buckling performance, and in particular, for understanding the role of anisotropy of the thermal expansion tensor due to curved fibers on the critical buckling temperature. In this work, this optimization problem is studied using a global representation of the fiber path, with the fiber described by two design variables β_0 and β_1. The stacking sequence is restricted to symmetric and balanced $[\pm\theta]_{ns}$. As an example, we investigate square panels that are simply supported and subjected to uniform temperature loading. The constitutive models are developed first, followed by buckling analysis of the out of plane equilibrium equation. The results are obtained numerically using an in-house finite element code for Eigen buckling analysis and validated with known results for straight fiber orientations. Next, fiber paths are varied and the optimum configuration to resist thermal buckling is found using gradient based optimization. Optimal fiber paths are then found for multiple material models and compared. One interesting outcome from a parametric study for different materials is the observed strong dependence of the critical buckling temperature on the thermal expansion ratio α_1/α_2 of the material.

2. Modeling

The constitutive relations for a thin laminate are based on classical lamination theory and are given in the form,

$$\begin{Bmatrix} N \\ M \end{Bmatrix} = \begin{bmatrix} A & B \\ B & D \end{bmatrix} \begin{Bmatrix} \varepsilon \\ \kappa \end{Bmatrix} \tag{1}$$

where the N and M vectors are the stress and moment resultants and ε and κ are the mid-plane strains and curvatures. The stiffness matrices are functions of panel position and are not constant. They are written compactly in the following form in terms of invariants [5]

$$[A,B,D] = \begin{bmatrix} e_{11} & e_{12} & e_{16} \\ e_{12} & e_{22} & e_{26} \\ e_{16} & e_{26} & e_{66} \end{bmatrix} \tag{2}$$

where

$$\begin{aligned} e_{11} &= U_1V_0 + U_2V_1 + U_3V_3, \\ e_{12} &= U_4V_0 - U_3V_3, \\ e_{16} &= -\frac{1}{2}U_2V_2 - U_3V_4, \\ e_{22} &= U_1V_0 - U_2V_1 + U_3V_3, \\ e_{26} &= -\frac{1}{2}U_2V_2 + U_3V_4, \\ e_{66} &= U_5V_0 - U_3V_3. \end{aligned} \tag{3}$$

The invariants for an orthotropic material, U_i, are shown in Appendix A. The form of V_i will change depending on the constitutive matrix. They are defined as,

$$\begin{aligned} V_{0(A,B,D)} &= \left[h, 0, \frac{h^3}{12}\right] \\ V_{1(A,B,D)} &= \int_{\frac{-h}{2}}^{\frac{h}{2}} cos(2\theta)[1,z,z^2]dz \\ V_{2(A,B,D)} &= \int_{\frac{-h}{2}}^{\frac{h}{2}} sin(2\theta)[1,z,z^2]dz \\ V_{3(A,B,D)} &= \int_{\frac{-h}{2}}^{\frac{h}{2}} cos(4\theta)[1,z,z^2]dz \\ V_{4(A,B,D)} &= \int_{\frac{-h}{2}}^{\frac{h}{2}} sin(4\theta)[1,z,z^2]dz \end{aligned} \tag{4}$$

where h is the total thickness of the laminate and θ is a function of position. For symmetric, balanced laminates the coupling stiffness matrix, the in-plane shear and normal coupling terms are eliminated; i.e. $B_{ij} = A_{16} = A_{26} = 0$. Now there is no in-plane/bending coupling and Eq. (1) is reduced to,

$$\begin{Bmatrix} M_x \\ M_y \\ M_{xy} \end{Bmatrix} = \begin{bmatrix} D_{11} & D_{12} & D_{16} \\ D_{12} & D_{22} & D_{26} \\ D_{16} & D_{26} & D_{66} \end{bmatrix} \begin{Bmatrix} \kappa_x \\ \kappa_y \\ \kappa_{xy} \end{Bmatrix} \tag{5}$$

Using Eqs. (2)–(5) the bending stiffness terms are defined by

$$\begin{aligned} D_{11} &= \frac{h^3}{12}(U_1 + U_2cos2\theta + U_3cos4\theta) \\ D_{12} &= \frac{h^3}{12}(U_4 - U_3cos4\theta) \\ D_{16} &= \frac{h^3}{12}\left(-\frac{1}{2}U_2sin2\theta - U_3sin4\theta\right) \\ D_{22} &= \frac{h^3}{12}(U_1 - U_2cos2\theta + U_3cos4\theta) \\ D_{26} &= \frac{h^3}{12}\left(-\frac{1}{2}U_2sin2\theta + U_3sin4\theta\right) \\ D_{66} &= \frac{h^3}{12}(U_5 - U_3cos4\theta) \end{aligned} \tag{6}$$

Note that the bending–twisting coupling terms are present.

2.1. Fiber path

For simplicity, fibers are made to vary along one of the coordinate directions. This analysis may easily be extended for fibers that vary along multiple coordinate axes. A linear variation along the x-coordinate axis is achieved by defining the fiber orientation as,

$$\theta(x) = \begin{cases} \frac{2(\beta_1-\beta_0)}{a}x + \beta_0 & \text{for } 0 \leqslant x < \frac{a}{2}; \\ \frac{2(\beta_0-\beta_1)}{a}x + \beta_0 & \text{for } -\frac{a}{2} \leqslant x < 0 \end{cases} \tag{7}$$

where a is the total length of the plate. The angle β_1 is fiber angle at the edges of the plate $(x = \pm\frac{a}{2})$, and β_0 is the angle of the fiber at the center of the plate $(x = 0)$. The path of the fiber that passes through the origin as a function of x is shown in Fig. 1. Here the origin is located at the geometric center of the plate with a fiber angle $\beta_0 = 60^\circ$, while the angle at edge is $\beta_1 = 20^\circ$.

3. Buckling analysis

For a simply supported symmetric balanced laminate, the Von Karman linearized out of plane buckling equation is given by,

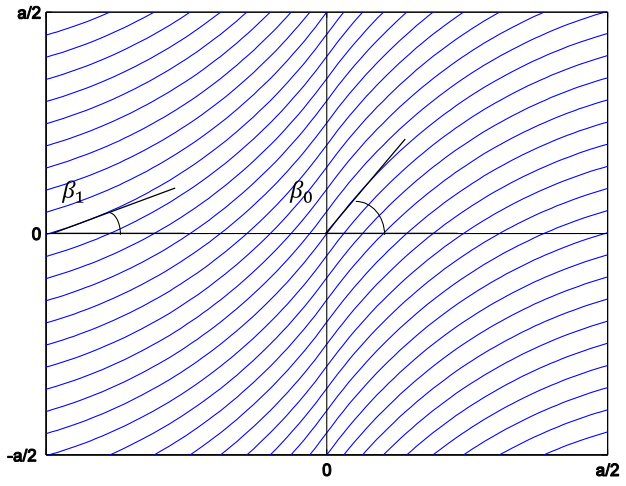

Fig. 1. Curvilinear fiber path for $\beta_1 = 20^\circ$ and $\beta_0 = 60^\circ$.

$$-N_x^i\frac{\partial^2 w}{\partial x^2} - N_y^i\frac{\partial^2 w}{\partial y^2} - 2N_{xy}^i\frac{\partial^2 w}{\partial x\partial y} + D_{11}\frac{\partial^4 w}{\partial x^4} + 2(D_{12}+2D_{16})\frac{\partial^4 w}{\partial x^2\partial y^2} + D_{22}\frac{\partial^4 w}{\partial y^4} + 4D_{16}\frac{\partial^4 w}{\partial x^3\partial y} + 4D_{26}\frac{\partial^4 w}{\partial y^3\partial x} = 0 \quad (8)$$

where w is the out of plane displacement. Entries denoted with superscript "i" correspond to the pre-buckled configuration. The presence of the bending-twisting coupling terms (D_{16}, D_{26}) in the Eq. (8) makes it difficult to assume a series solution in solving this equation; therefore, the finite element method is used. For the finite element formulation, the discretized domain will produce locally straight, constant angle, fiber paths; each element will have a local fiber angle associated with it. Therefore, we model the global fiber orientation angle as a linear piecewise function. For this treatment, the local angle $\bar{\theta}$ is calculated by taking the elemental average of the angle θ (Eq. (7)). The local element laminate layup is then assumed to be $[\pm\bar{\theta}]_{ns}$. Now the stiffness matrices (A, B, D) are constant for each element. This process is shown in Fig. 2 below. For an angle-ply laminate with prescribed constant thermal load ΔT, the pre-buckled loads are easily found using classical lamination theory, as,

$$\begin{aligned} N_x^i &= -\Delta T(A_{11}\alpha_{11} + A_{12}\alpha_{22}) \\ N_y^i &= -\Delta T(A_{12}\alpha_{11} + A_{22}\alpha_{22}) \\ N_{xy}^i &= 0 \end{aligned} \quad (9)$$

The critical buckling temperature ΔT_{crit} is determined using the following eigenvalue problem,

$$|K_M + \lambda K_G| = 0 \quad (10)$$

where the smallest eigenvalue λ_{min} corresponds to the critical buckling temperature ΔT_{crit}. The material stiffness matrix K_M and the geometric stiffness matrix K_G are found using Galerkin method and are stated in Appendix B. This formulation uses 4-noded Kirchhoff plate elements [17] with degrees of freedom w, $\partial w/\partial x$, and $\partial w/\partial y$.

4. Validation

4.1. Isotropic plate

A convergence study and method validation is presented for an isotropic aluminum plate. Fig. 3 shows the critical buckling temperature of an aluminum plate as a function of the ratio a/h. The results from the method described above are compared with the analytical solution found in reference [14]. A 400 element mesh is within a tolerance of 10^{-2} and will be used for all future analysis. Denser meshes are not considered due to their computational expense, especially during optimization where gradients are calculated with finite differences.

4.2. Cross-ply layup

In this section, a composite four layer cross-ply layup $[0/90]_s$ is considered. The angles β_0 and β_1 are equal for straight fiber configurations. The critical buckling temperature found in reference [15]

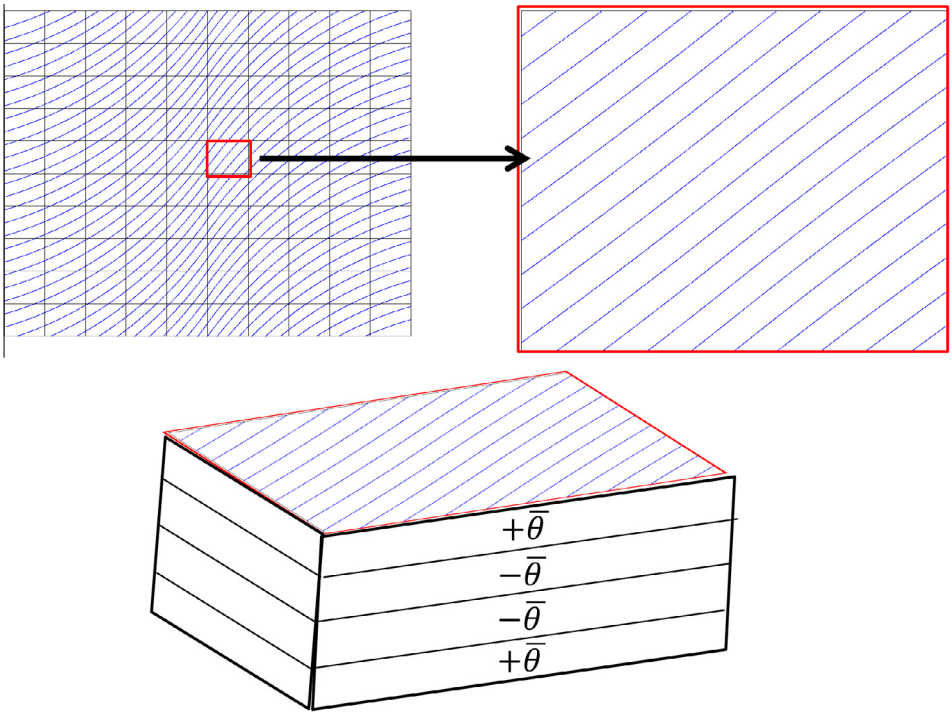

Fig. 2. Curvilinear fiber path is approximated constant from each element.

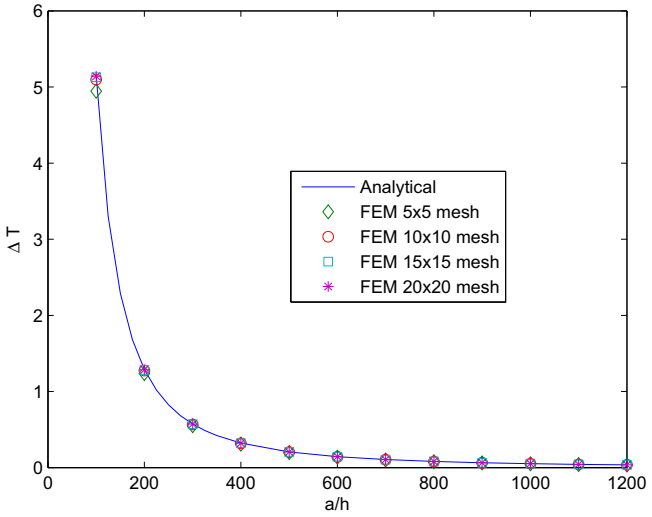

Fig. 3. Exact and FEM solutions for critical buckling temperature of aluminum plate vs a/h.

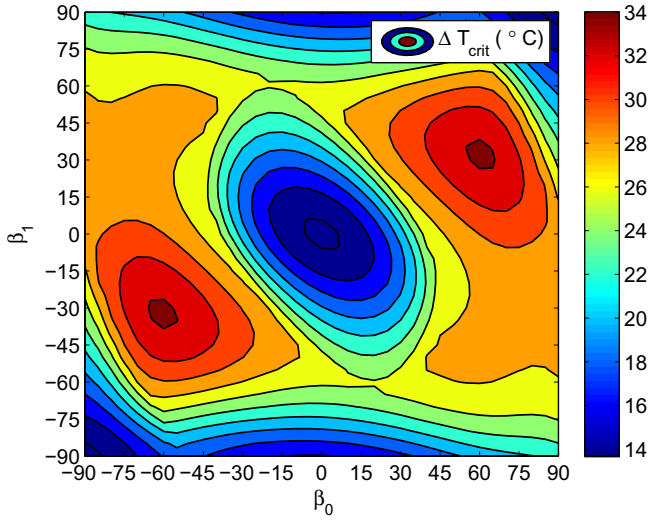

Fig. 4. Temperature contour as a function of fiber angles for Graphite/Epoxy.

is $\Delta T_{crit} = 0.0996$ °C. This work predicts a buckling temperature of $\Delta T_{crit} = 0.0996$ °C and is in good agreement with the work cited.

4.3. Angle-ply layup

Next a Graphite/Epoxy angle-ply layup is considered. Material properties are given in Appendix C where $a = 0.15$ m and the $h = 1.016$ mm. Again the angles β_0 and β_1 are equal and for a angle-ply layup $\beta_0 = \beta_1 = \theta$. For a four layer angle-ply layup this work predicts an optimal configuration of $[\pm 45]_s$ which can be found as the optimal configuration to resist thermal buckling in other works [2,3].

4.4. Complex layup

For the final case, a complex layup of $[+45/-45/0/90]_s$ is considered. The same geometry and materials are used from the previous example. Results obtained numerically by a Rayleigh–Ritz formulation results in a critical buckling temperature of $\Delta T_{crit} = 38.6$ °C [2]. This work predicts a higher critical buckling temperature of $\Delta T_{crit} = 39.4$ °C. Results from this section validate this method and analysis is continued with confidence. Now the fiber path is varied spatially for the same Graphite/Epoxy composite.

5. Results

5.1. Graphite/Epoxy composite

The critical buckling temperature for multiple configurations is found by performing an exhaustive search; the angles β_0 and β_1 are equally varied from -90° to 90°. A contour plot of the critical buckling temperature ΔT_{crit} as a function of the fiber angles β_0 and β_1 is shown in Fig. 4. These results show a temperature profile that contains multiple maxima and minima. Here, a diagonal across the figure represents a straight angle configuration ($\beta_0 = \beta_1 = \theta$), where the straight angle configuration with the largest resistance to thermal buckling is $[\pm 45]_s$ corresponding to $\Delta T_{crit} = 32.45$ °C. As expected the lowest critical buckling temperature corresponds to a $\beta_1 = \beta_0 = 0$ orientation where all fibers are aligned in one direction, giving little buckling resistance in the direction perpendicular to the fibers. The temperature profile is symmetric about the $\beta_1 = -\beta_0$ line; therefore, the profile is not unique over -90° to 90° domain and $\Delta T(\beta_0, \beta_1) = \Delta T(-\beta_0, -\beta_1)$. Although Fig. 4 shows a complex temperature profile with multiple local maximums, it is obvious that a strong maximum exists. Finding the optimal fiber configuration that resists thermal buckling is a multi-variable optimization problem. A quasi-Newton method [18] is implemented to find the maxima efficiently by maximizing ΔT_{crit} with respect to β_0 and β_1. Sensitivities are calculated using finite differences with a step size of 10^{-7}. The initial angle configuration is an angle-ply layup of $[\pm 45]_s$. The optimal configuration is given by $\beta_0 = 60.70^\circ$ and $\beta_1 = 32.19^\circ$ corresponding to the maximum critical buckling temperature of $\Delta T_{crit} = 34.26$ °C. Theses values, obtained through optimization, are in good agreement with Fig. 4 and give a 5.6% increase in thermal buckling load when compared to the optimum straight fiber configuration of $[\pm 45]_s$.

5.2. Angle optimization for multiple materials

Next, analysis is performed on multiple composite materials in an effort to further improve on percent increase of critical buckling temperature. Material constants are shown in Appendix C. A global search is performed and the resulting temperature profiles for each material are shown on Fig. 5. As expected, the profiles are symmetric about the $\beta_1 = -\beta_0$ line. All temperature profiles show strong local minima. Optimal results for these materials are reported on Table 1. Values on Table 1 are in agreement with the contours shown in Fig. 5. The largest increase in critical buckling temperature is for Carbon/Epoxy where there is a 36.9% increase in buckling temperature for $\beta_1 = 69.0^\circ$ and $\beta_0 = -5.71^\circ$. Interestingly, since the fiber angle in not restricted, the optimal angle at the edge of the plate is negative (Fig. 6) or greater than 90°. This is also the case for the Boron/Epoxy (Fig. 7) where the optimal angle at the center of the plate is negative. These result show that varying the fiber angle spatially provides a significant increase to resisting thermal buckling. The ratio a/h is varied for each material and results are plotted on Fig. 8. Results follow the same trend as those for the isotropic plate in Fig. 3. As the ratio a/h increases, the critical buckling temperature decreases. For smaller ratios the Carbon/Polyimide provides the highest resistance to thermal buckling while the S-Glass/Epoxy results in the lowest. All other materials fall in between. As the ratio a/h increases, the critical buckling temperature decays and the materials are almost indistinguishable. It should be noted that varying the ratio a/h has no effect on the optimal fiber angles β_0, β_1. Note that this work does not include postbuckling effects or imperfection analysis which may contribute to discrepancies of the actual reported buckling temper-

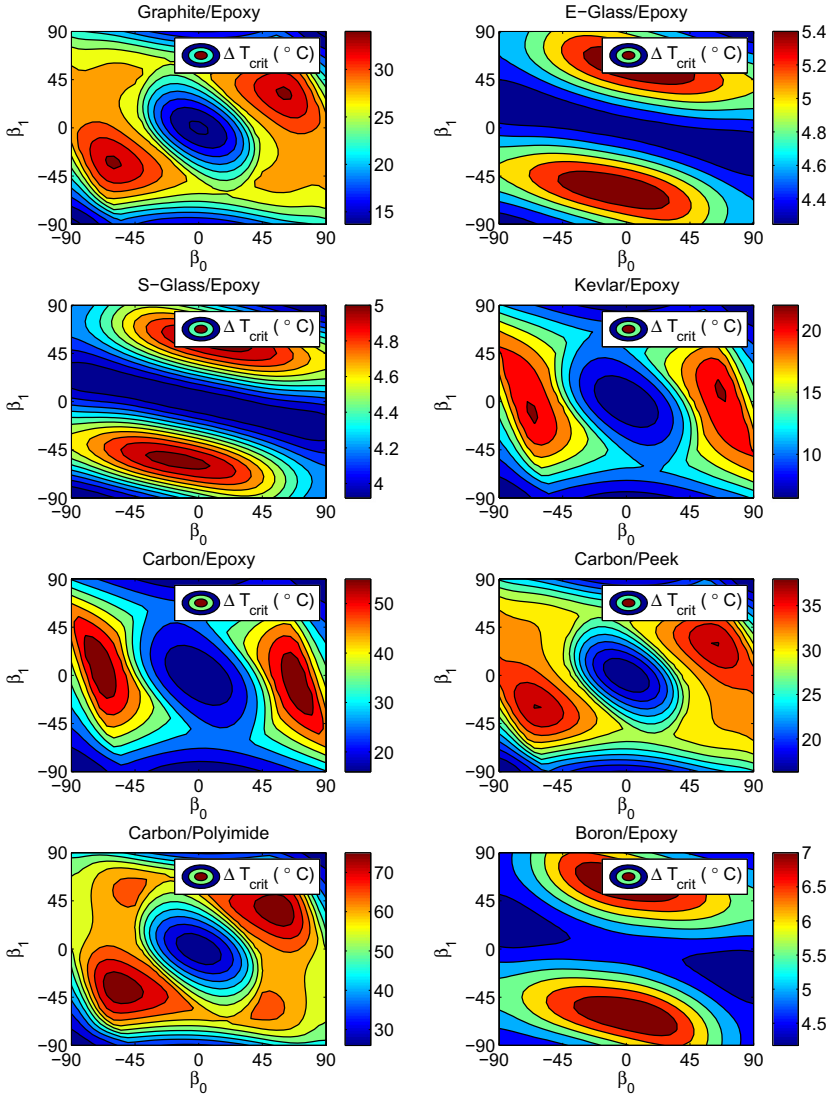

Fig. 5. Temperature contour as a function of fiber angles for multiple materials.

Table 1
Optimization of fiber angle path for multiple materials.

Material	β_0 (°)	β_1 (°)	ΔT_{crit}(°C)	$[\pm 45]_s$ % increase
E-Glass/Epoxy	6.710	58.04	5.58	2.8
S-Glass/Epoxy	16.12	54.74	5.04	1.6
Kevlar/Epoxy	66.05	11.73	22.18	24.1
Carbon/Epoxy	69.00	−5.705	57.79	36.9
Carbon/Peek	63.07	29.50	38.08	7.3
Carbon/Polyimide	56.30	36.68	78.28	2.9
Boron/Epoxy	−6.57	63.28	7.50	10.9

atures with experiments. Inclusion of these mechanisms are beyond the scope of this paper. Although the values of the critical buckling temperature may differ from experiments, the optimal fiber path or configuration may not. An example of this is the work done by Ashton and Love [19] where the buckling values for composite plates are over predicted by theory but the trends of the critical buckling load versus fiber angles are similar.

5.3. Varying coefficients of thermal expansion

Although E-Glass/Epoxy and S-Glass/Epoxy have similar material properties, their optimal fiber paths vary. This implies that the optimum fiber path is extremely sensitive to certain material properties; slightly perturbed material properties produce different fiber paths. It is apparent that there is a heavy influence from

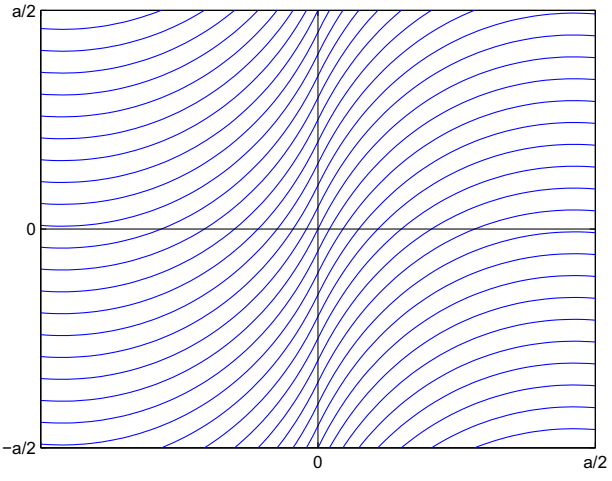

Fig. 6. Optimum fiber path for Carbon/Epoxy.

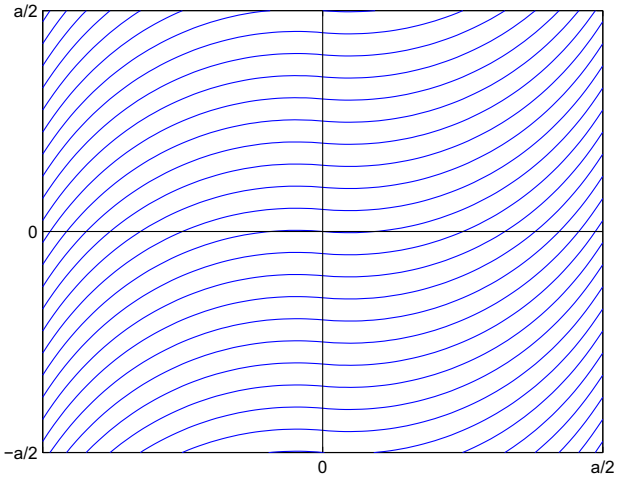

Fig. 7. Optimum fiber path for Boron/Epoxy.

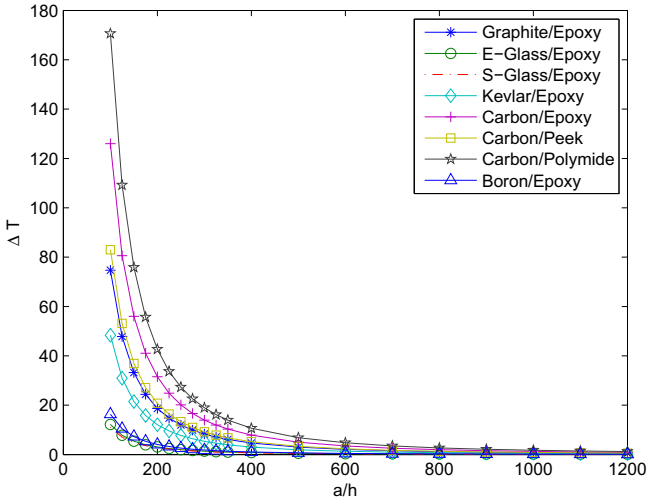

Fig. 8. Critical buckling temperature of a square laminate versus a/h for multiple materials.

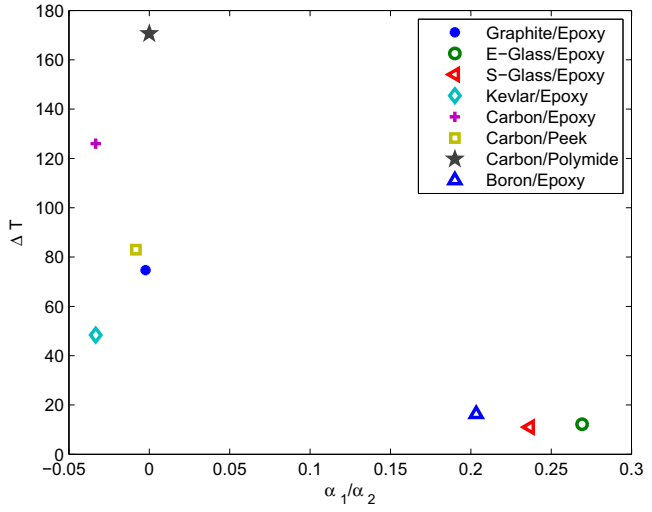

Fig. 9. Critical buckling versus α_1/α_2 for $a/h = 100$.

the coefficients of thermal expansion on the critical buckling temperature. Fig. 9 plots the critical buckling temperature versus the ratio α_1/α_2 for an aspect ratio $a/h = 100$. Negative thermal expansion ratios give a higher resistance to thermal buckling while positive values of this ratio produce lower critical buckling temperatures. This plot is in agreement with results from Fig. 8, where Carbon/Polyimide provides the highest resistance to thermal buckling. To study this effect, the initial thermal expansion coefficient ratio of Graphite/Epoxy is increased with all other material properties fixed. Fig. 10 shows that as the thermal expansion ratio increases, the critical buckling temperature decreases. As increasing expansion ratio approaches the thermal expansion ratio of Boron/Epoxy the critical buckling temperatures differ by 4.26 °C suggesting influences from other material properties. Fig. 11 shows the effect of the thermal expansion ratio on the optimum fiber path. As α_1/α_2 increases, β_0 decreases and become negative reaching a final value of $-15.06°$. Alternatively, β_1 increases and reaches the final value of 70.91°. These optimum angle values are closer to the values reported for Boron/Epoxy on Table 1. Again the gap between these values can be attributed to the influence of the other material properties.

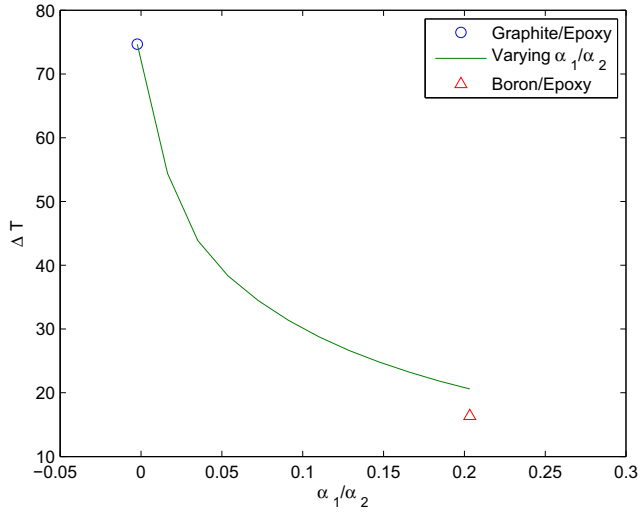

Fig. 10. Effect of increasing α_1/α_2 on ΔT.

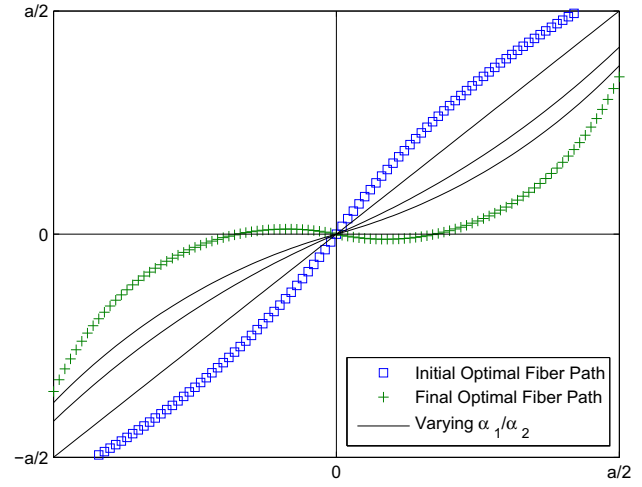

Fig. 11. Effect of increasing α_1/α_2 on the optimum fiber path.

Table C.2
Material properties.

Material	E_1(GPa)	E_2(GPa)	G_{12}(GPa)	v_{12}
Graphite/Epoxy	155	8.07	4.55	0.22
E-Glass/Epoxy	41	10.04	4.3	0.28
S-Glass/Epoxy	45	11.0	4.5	0.29
Kevlar/Epoxy	80	5.5	2.2	0.34
Carbon/Epoxy	147	10.3	7.0	0.27
Carbon/Peek	138	8.7	5.0	0.28
Carbon/Polyimide	216	5.0	4.5	0.25
Boron/Epoxy	201	21.7	5.4	0.17

Table C.3
Coefficients of thermal expansion.

Material	$\alpha_1(^\circ C^{-1})E-6$	$\alpha_2(^\circ C^{-1})E-6$
Graphite/Epoxy	−0.07	30.1
E-Glass/Epoxy	7.0	26
S-Glass/Epoxy	7.1	30
Kevlar/Epoxy	−2.0	60
Carbon/Epoxy	−0.9	27
Carbon/Peek	−0.2	24
Carbon/Polyimide	0.0	25
Boron/Epoxy	6.1	30

6. Conclusions

Thermal buckling of composite plates with spatially varying fiber orientations have been investigated. In this work, square plates with simply supported boundary conditions, subjected to uniform temperature distribution, were considered. Optimization of the thermal buckling load was performed for multiple material models with respect to two fiber path parameters. It was found that curved fiber angle orientations provided better resistance to thermal buckling than straight fiber configurations in all cases. For the Carbon/Epoxy composite the optimal configuration obtained from this analysis provides a 36.9% increase to critical buckling temperature over the straight angle fiber configuration of $[\pm 45]_s$. Optimal buckling temperatures and fiber paths were investigated for various coefficients of thermal expansion combinations. It was found that there is a strong dependence on the ratio α_1/α_2. Future work includes experimental validation of these results and extension of numerical methods to investigate three-dimensional fiber paths and for composite rectangular plates with varying layups.

Appendix A. Orthotropic invariants

The invariants for an orthotropic material are given as

$$U_1 = \frac{3Q_{11} + 3Q_{22} + 2Q_{12} + 4Q_{66}}{8}$$

$$U_2 = \frac{Q_{11} - Q_{22}}{2}$$

$$U_3 = \frac{Q_{11} + Q_{22} - 2Q_{12} - 4Q_{66}}{8} \tag{A.1}$$

$$U_4 = \frac{Q_{11} + Q_{22} + 6Q_{12} - 4Q_{66}}{8}$$

$$U_5 = \frac{Q_{11} + Q_{22} + 2Q_{12} - 4Q_{66}}{8}$$

where

$$Q_{11} = \frac{E_{11}}{1 - v_{12}v_{21}}$$

$$Q_{12} = \frac{v_{12}E_{22}}{1 - v_{12}v_{21}} \tag{A.2}$$

$$Q_{22} = \frac{E_{22}}{1 - v_{12}v_{21}}$$

$$Q_{66} = G_{12}$$

Appendix B. Stiffness matrices

The material stiffness matrix is given by

$$K_M = \int_y \int_x [S]^T [D][S] t dx dy \tag{B.1}$$

where t is the element thickness, D is the bending stiffness matrix (Eq. (6)) and

$$S = \begin{Bmatrix} \partial^2/\partial x^2 \\ \partial^2/\partial y^2 \\ 2\partial^2/\partial x \partial y \end{Bmatrix} [\phi] \tag{B.2}$$

Here, the ϕ matrix is the shape functions corresponding to a 4-node Kirchhoff plate element. The geometric stiffness matrix is given by

$$K_{Gij} = \int_y \int_x \left[\phi_x^i \frac{\partial \phi_i}{\partial x}\frac{\partial \phi_j}{\partial x} + \phi_y^i \frac{\partial \phi_i}{\partial y}\frac{\partial \phi_j}{\partial y} + \phi_{xy}^i \left(\frac{\partial \phi_i}{\partial x}\frac{\partial \phi_j}{\partial y} + \frac{\partial \phi_i}{\partial y}\frac{\partial \phi_j}{\partial x} \right) \right] t dx dy \tag{B.3}$$

Appendix C. Material properties

Material and thermal properties are given on Tables C.2 and C.3 [16].

References

[1] Rangarajan A, D'Mello RJ, Sundararaghavan V, Waas AM. Minimization of thermal expansion of symmetric, balanced, angle ply laminates by optimization of fiber path configurations. Compos Sci Technol 2011;71(8):1105–9.

[2] Meyers CA, Hyer MW. Thermally-induced, geometrically nonlinear response of symmetrically laminated composite plates. Compos Eng 1992;2(1):3–20.

[3] Walker M, Reiss T, Adali S, Verijenko VE. Optimal design of symmetrically laminated plates for maximum buckling temperature. J Therm Stresses 1997;20(1):21–33.

[4] Gürdal Z, Olmedo RA. Composite laminates with spatially varying fiber: variable stiffness panel concept. Proceedings of the AIAA/ASME/ASCE/AHS 33rd structures, structural dynamics and materials conference, vol. 2. AIAA; 1992 [p. 798–808].

[5] Olmedo RA, Gürdal Z. Buckling response of laminates with spatially varying fiber orientations, AIAA/ASME/ASCE/AHS/ASC 34th structures, structural dynamics and materials conference, and AIAA/ASME adaptive structures Forum, La Jolla, CA, Apr. 19–22, 1993, Technical Papers. Pt. 4 (A93-33876 13–39), p. 2261–2269.

[6] Lopes CS, Camanho PP, Gürdal Z. Variable-stiffness composite panels: effects of stiffness variation on the buckling and failure responses. In: 7th EUROMECH solid mechanics conference. Lisbon, Portugal, Sep. 7–11, 2009.

[7] Gürdal Z, Tatting BF, Wu CK. Variable-stiffness composite panels: effects of stiffness variation on the in-plane and buckling response. Compos Part A Appl Sci Manuf 2008;39(5):911–22.

[8] J Groh RM, Weaver PM. Buckling analysis of variable angle tow, variable thickness panels with transverse shear effects. Compos Struct 2014;107:482–93.

[9] Jegley DC, Tatting BF, Gürdal Z. Optimization of elastically tailored tow-placed plates with holes. In: Proceedings of the AIAA/ASME/ASCE/AHS/ASC 44th structures, structural dynamics and materials conference. Norfolk, VA, Apr. 2003, p. 2003–1420.

[10] Hyer MW, Charette RF. Use of curvilinear fiber format in composite structure design. AIAA J 1991;2(6):1011–5.

[11] Nagendra S, Kodiyalam S, Davis JE. Optimization of tow fiber paths for composite design. In: Proceedings of the 36th AIAA/ASME/ASCE/AHS/ASC structures, structural dynamics and materials (SDM) conference. New Orleans, LA. Apr. 1995.

[12] Setoodeh S, Abdalla MM, IJsselmuiden ST, Grdal Z. Design of variable-stiffness composite panels for maximum buckling load. Compos Struct 2009;87(1):109–17.
[13] IJsselmuiden ST, Abdalla MM, Gürdal Z. Optimization of variable-stiffness panels for maximum buckling load using lamination parameters. AIAA J 2010;48(1):134–43.
[14] Brush DO, Orr D, Almroth BO. Buckling of bars, plates, and shells, vol. 6. New York: McGraw-Hill; 1975 [p. 384–5, Issue 6].
[15] Kant T, Babu CS. Thermal buckling analysis of skew fibre-reinforced composite and sandwich plates using shear deformable finite element models. Compos Struct 2000;49(1):77–85.
[16] Daniel IM, Ishai O. Engineering mechanics of composite materials. New York: Oxford University Press; 2006.
[17] Cook RD, Malkus DS, Plesha ME, Witt RJ. Concepts and applications of finite element analysis. John Wiley and Sons; 2007.
[18] Fletcher R, Powell MJ. A rapidly convergent descent method for minimization. Comput J 1963;6(2):163–8.
[19] Ashton JE, Love TS. Experimental study of the stability of composite plates. J Compos Mater 1969;3(2):230–42.